Effect of Increased Mechanical Strength on the Machinability of Graphite Cast Irons in Face Milling

Alcione dos Reis
Leonardo R Ribeiro da Silva (leonardo.rrs@gmail.com)
Universidade Federal de Uberlandia https://orcid.org/0000-0003-2777-4500
Aline Elias da Silva
Lucas Melo Queiroz Barbosa
Álisson Rocha Machado
Cássio Luiz Francisco de Andrade
Wilson Luiz Guesser

Research Article

Keywords: Cast iron machinability, Microstructural characteristics, Face milling, Tool wear, Surface roughness

Posted Date: November 17th, 2022

DOI: https://doi.org/10.21203/rs.3.rs-2234473/v1

Version of Record: A version of this preprint was published at The International Journal of Advanced Manufacturing Technology on February 4th, 2023. See the published version at https://doi.org/10.1007/s00170-023-11012-0.

Abstract

Due to the low cost and high vibration damping capacity, gray cast irons are commonly used in machine tool bases, in addition to applications with noise restrictions, such as engine blocks, housings, and brakes. The matrix's graphite, sulfides, and ferrite/pearlite ratio are some of the most important parameters governing the machinability of the gray cast irons. This work aims to evaluate the machinability of high-resistance gray cast irons of the FC 300 grade, in two versions, with the addition of molybdenum (FC 300 $_{(Mo)}$) and with refined graphite and addition of molybdenum (FC 300 $_{(Mo+RG)}$), for use in cylinder heads and engines blocks, compared to materials that have been used for this purpose, gray cast iron FC 250 and the compacted graphite cast iron FV450. The face milling process was chosen for the tests, as it is widely used in manufacturing cylinder heads and engine blocks. Uncoated cemented carbide tools with tangential rhomboid geometry were used in the experiments. Analysis of tool life and wear mechanisms and machined surfaces' quality (Ra roughness parameter) where the output variables are considered. The materials were characterized according to the cementite interlayer spacing and microhardness of the perlite matrix, the number of eutectic cells, and the distribution of manganese sulfide inclusions, with those characterizations being correlated with the machinability results. The cutting speed and feed were varied, and the dry condition was used. Among the gray cast irons investigated, the FC 300$_{(Mo+RG)}$ presented worse machinability rates because of its greater mechanical resistance and hardness. Regarding the surface finish, at the beginning of the tool life tests (without considering tool wear) and employing the highest cutting speed, the FC 300$_{(Mo+RG)}$ showed the best results, but at the lowest cutting speed, the worst.

1. Introduction

Stricter regulations on gas emissions have led car manufacturers to explore different vehicle engine options. Currently, to improve performance in the manufacture of cylinder blocks and cylinder heads of high-powered diesel engines, as well as other castings, a certain number of alloying elements are generally added to gray cast iron. Cast iron grade FC300 materials are widely used to manufacture various industrial products. The reasons are good castability, machinability, and abrasion resistance, and its vibration-dampening capacity is much higher than that of light steels [1, 2, 3]. Given this, the mechanical resistance of cast iron, that is, their ability to withstand external stresses without causing them to cause plastic deformations, and consequently their grades, are conditioned to their final structure obtained [4, 5].

Therefore, this property depends on the shape and amount of graphite and the amount of ferrite and/or perlite in the metallic matrix, in which the resistance is increased with higher levels of perlite and the reduction of the interlayer spacing of the perlite. [5, 6, 7].

The usual mechanism for increasing the tensile strength and hardness of gray cast irons is the addition of alloying elements, such as chromium (Cr), molybdenum (Mo), tin (Sn), and copper (Cu). Additional amounts of copper and tin (pearlized elements) promote the refining of the pearlite or reduction of interlayer spacing, which results in increased strength. On the other hand, Chromium and molybdenum act in the formation of carbides, and, like Sn and Cu, Mo can also be used as a perlite refiner [8, 9].

To achieve a minimum tensile strength of 300 MPa, the carbon content is also reduced from 3.2 to 3.0%, which results in smaller graphite lamellae, thus reducing the risk of starting and crack propagation. In this way, a 10 to 20% increase in mechanical properties is achieved from this [10, 11].

The addition of alloying elements depends on the elemental composition and manufacturing method to provide the desired mechanical properties. Therefore, reducing or eliminating Cu use by technical measures without reducing the mechanical properties and processability in mass production will bring some economic and technological benefits [12, 13].

The study on machinability, cutting strategies, and application technology of gray cast iron is today a priority in large companies and research institutions worldwide, becoming an effective guarantee for high-quality products [14].

Gray cast iron has become a popular material among other cast metals, being widely applied in modern industrial production, mainly for its low cost (20 to 40% less than steel), in addition to having a wide variety of mechanical properties achievable, as good castability, machining property convenient and good wear resistance [15, 16]. The microstructure of gray cast iron is characterized by graphite lamellas dispersed in the ferrous matrix. The casting practice can influence the nucleation and growth of graphite flakes so that the size and type improve the desired properties. The quantity and size of graphite, morphology, and distribution of these lamellae are critical in determining the mechanical behavior of gray cast iron [15, 17].

According to Guesser [9], the machinability of gray cast irons increases as you move towards higher strength grades due to the increased abrasiveness with the increase in the amount of perlite in the matrix and due to the decrease in lubricating action and consequent reduction in ease chip breaking with a decrease in the amount of graphite.

Another way to evaluate the machinability of cast iron is by combining the hardness test with an evaluation of microstructure due to some microconstituents that adversely affect machinability (ASM). Thus, it is emphasized that the microstructure plays a crucial role in altering the mechanical properties of any material [18]. Controlling the microstructure, optimizing the process parameters, and adding alloy elements are highly necessary [18, 19]. The main constituent elements of cast iron are mainly carbon, phosphorus,s and silicon, among others. The presence of silicon and phosphorus determines the solubility of carbon in the molten metal [20]

Silicon is one of the essential elements in producing gray cast iron because it is a stabilizing element of graphite. Thus, it promotes graphite development at the site of iron carbides. It is verified from the experience that the Si content of around 3% restricts the formation of iron carbide because no carbon is left in the chemical form [21].

Adding nickel refines the pearlite structure and graphite gray cast iron, improving strength and hardness to balance the differences in thick sections. High hardness, like that of white cast iron bars, produced by adding sodium chloride salt to gray cast iron, is recommended for wear resistance [22, 23].

As for molybdenum, this is a carbide-forming element used to strengthen and harden iron because of the transformation of austenite into fine perlite and bainite, generally added in gray cast iron to refine perlite [24,

25, 26]. Molybdenum is not a promoter of perlite; however, it is usually added as a ferromolybdenum containing 60 to 70% (Mo) [27, 28]. Copper and molybdenum in gray cast iron guarantee greater hardness and tensile strength than the common pearlitic types of gray cast iron [11].

The gray cast irons of FC300 class possess good mechanical properties, where combinations of multiple structures with low silicon content, fine graphite, and perlite make them stronger and increase their resistance [29, 30]. The combination of microstructure with graphite reinforcement and excellent mechanical strength has led the cast iron alloys of the FC300 class to be used in a wide range of industrial applications, such as automotive parts, internal combustion engines, piping systems, and construction parts [31].

However, compared with conventional FC250 and FC300, the class is considered a lower-cut material. The problems encountered during the machining of the FC300 class are caused by changes in the microstructure formation due to the addition of alloying elements [29, 31]. This is an issue to be considered in industrial environments because it becomes difficult to predict the actual tool life and to specify the most suitable cutting conditions for a given cast alloy.

The integrity of the surface is directly related to the quality achieved in the final machining, which strongly affects the product's performance. Among the factors that can influence the quality of the product's surface are the cutting speed, the feed, the depth of cut, the geometry of the tool, the wear of the tool, and the properties of the part [29, 32].

In practice, machining operations can only fully develop the potential of machine tools and cutting tools after optimizing the cutting parameters to obtain the best work efficiency and tool life [33, 34].

The present study aims to evaluate the influence of the microstructure on the machinability of gray high-strength cast iron, of the FC300 class, for use in diesel engine blocks and heads. For this purpose, two versions of FC300 gray cast iron were produced, one with graphite refining (FC 300 (RG)) and the other, which in addition to graphite refining, has molybdenum addition (FC 300 (Mo + RG)). The FC250 gray cast iron and vermicular iron FV450 were also investigated for comparison purposes. These materials were machined in the front milling, with carbide tools, with comparisons of the tool life and the surface roughness of the part, considering in the analysis and discussions of the results the microstructural characteristics of the materials.

2. Materials And Methods

2.1. Materials characterization

The materials tested through the face milling process were the high-strength gray cast iron FC 300 $_{(Mo),}$ which has molybdenum as an alloying element, the FC 300 $_{(Mo + RG),}$ which also has molybdenum as an alloying element, as well as graphite refinement, the gray cast iron FC 250 and the compressed graphite cast iron FV 450. The last two will be investigated to serve as references in the comparisons.

The micrographs of the materials were obtained using a scanning electron microscope (SEM - Hitachi TM 3000) as well as the micrographs showing 100% pearlitic matrix in both, obtained by optical microscopy (Olympus microscope), this being a technique used to view a sample close up with the magnification of a lens

with visible light. Figure 1 shows the distribution of the graphites of the investigated materials. The graphite morphology was evaluated using scanning electron microscopy (SEM), and the pearlitic matrix using optical microscopy after etching with Nital (3%). The chemical composition, mechanical properties, and characteristics of the matrix and graphite of the materials were made available by the manufacturer [7] and detailed in Table 1 and Table 2.

Table 1
Chemical composition of the evaluated materials [7].

Material	Si [%]	Mn [%]	P [%]	S [%]	Cr [%]	Ti [%]	Sn [%]	Cu [%]	Mo [%]	Ni [%]	Cu eq.
FC 250	1.900 - 2.000	0.500 - 0.600	0.020 - 0.030	0.100	0.270	0.01-	0.130	0.280	0.020	-	2.38
FC 300 (Mo)	2.11	0.50	0.036	0.10	0.23	0.01	0.06	0.67	0.23	-	4.07
FC 300 (Mo+RG)	2.12	0.66	0.035	0.10	0.23	0.01	0.06	0.67	0.22	-	4.12
FV 450	2.210	0.320	0.019	0.003	0.031	0.007	0.070	0.990	-	0.016	-

Table 2
Characteristics of graphite and matrix of the materials [7].

Material	Matrix	Graphite	
		Form	% Nodularity
FC 250	100% Pearlitic	I	-
FC 300 (Mo)	100% Pearlitic	I	-
FC 300 (Mo+RG)	100% Pearlitic	I	-
FV 450	99% Pearlitic	III - VI	9

The metallographic analysis allowed us to observe the appearance of graphite in the three gray irons as thin and uniform flakes with random orientation, typical of form I and type A [8]. In the compacted graphite cast iron, the shapes observed as graphite III and VI correspond, respectively, to the form of worms and nodules, as shown in Fig. 1d. For all the materials, this information about the metallography of gray cast iron is crucial for analyzing the machining results since the number of eutectic cells reflects directly on the volume and size of the graphites. A larger number of cells tend to have a thinner structure with a smaller graphite size, which reduces the crack propagation condition, making machining difficult. Table 3 shows the Brinell hardness of the materials, the Vickers microhardness of the pearlite, and the mechanical strength of all the tested materials.

Table 3
Hardness and tensile strength of the evaluated materials [7].

Properties	FC 250	FC 300 $_{(Mo)}$	FC 300 $_{(Mo+RG)}$	FV 450
Hardness [HB]	187	207	217	229
Pearlite microhardness [HV]	278	291	313	364
Ultimate tensile strength [MPa]	259	278	283	524

To determine the amount of manganese sulfide inclusions (MnS/mm^2), for each cast iron sample, ten images at a magnification of (500x) were used, and for area evaluation, 150 particles of manganese sulfide were randomly selected from the images. Figure 2 (a) shows examples of the measured particle areas.

The cementite interlayer spacing of the perlite was determined by etching the samples with 3% Nital reagent. Twenty-five images were taken at a magnification of 20000x by scanning electron microscopy of different regions, with 25 points being selected at random to measure the intersections of the cementite lamellae according to the methodology established by Vander Voort and Roosz [9].

2.2. Material samples, cutting toolS, and milling TESTS

The work materials were supplied by TUPY S.A [7] in the form of rectangular bars whose dimensions were approximately 400 mm long, 240 mm wide, and 40 mm thick. Before the face milling tests, the specimens had their surfaces pre-machined. This process was employed to remove residues from the sand-casting process and the chill zone, as both can increase the tool wear, masking the influence of the input parameters.

The cutting tools used in this research were uncoated cemented carbide inserts manufactured by Walter Tools, ISO code - LNHU130608R-L55T Tiger-tec® Silver, grade WKP 25S. These inserts have a double-sided tangential rhomboid geometry suitable for finishing. These tools were mounted on a 90 ° angle cutter head, BLAXX model, code F5141.B27.080.Z10.12, with a diameter of 80 mm and capacity for ten inserts, also manufactured by Walter Tools. Figure 3 and the table shows the details of the tools used in the experiments. Only one insert was mounted in the milling cutters for the trials, which according to Richetti, et al. [10], does not compromise the comparative results.

Table 4
The geometry of the tool used in the tests.

Description	Symbol	Value
Indexable insert tolerance class		H
Number of cutting edges		4
Indexable insert width	l_2	12 mm
Cutting edge length	l	13 mm
Insert thickness	s	6.8 mm
Corner radius	r	0.8 mm
Wiper cutting-edge length	b	2.2 mm

The tool life tests followed a factorial design of experiments (DOE) of 2^3, with two quantitative variables (cutting speed, v_c; feed rate, f) and a qualitative variable (workpiece material). The high (+) and low (-) levels of the variables are shown in Table 5. In a predominantly concordant milling cutting, the axial depth of cut (ap) and the radial depth of cut (ae) remained constant at 1 mm and 60 mm, respectively. To guarantee statistical reliability, all tests were repeated twice, totaling three tests in each condition (test and two replicates).

Table 5
Levels of the design of the experiments used in the tests.

Level	v_c [m/min]	f [mm/rev]	Work material
(+)	350	0,2	FC 250
(-)	230	0,1	FC 300 $_{(Mo)}$; FC 300 $_{(Mo+RG)}$; FV 450

The levels of the input variables were defined to provide a tool life suitable for the carbide inserts so that they were not too long (at low levels), consuming much time and material, nor too short (at high levels), offering little information about the test. As the qualitative variable (material of the workpiece) has 4 levels, instead of 8 tests, 16 were necessary, totaling 48 tests with repetitions.

The tests were carried out under dry conditions, in a vertical CNC machining center Discovery model 760, with main spindle power of 11 kW and a maximum rotation of 10 000 RPM, from the manufacturer ROMI - Bridgeport. For the tool life tests, maximum flank wear (VB_{Bmax}) equal to 0.40 mm was used as the end-of-tool life criterion. At the end of each run, the tool wear and surface roughness of the workpiece was measured. After reaching the end of their lives, the tools had their wear mechanisms evaluated by scanning electron microscopy.

To measure the surface roughness parameters (Ra) was used a portable roughness meter, model SJ201 P / M from MITUTOYO. This instrument has a needle probe with a 2 µm diamond tip radius and 0.1 µm resolution. A 0.8 mm cut-off filter was used, following the recommendation of the /ISO 4288 standard [11].

3. Results And Discussions

3.1. Distribution of MnS particles and pearlite interlayer spacing

The results of the average amount of MnS inclusions/mm² and the average area of these inclusions in the gray cast iron are shown in Fig. 4. The vermicular cast iron, in turn, does not present MnS inclusions in its microstructure since sulfur is reduced in these materials. Figure 4a shows slight differences in the averages of these particles. The cast iron with graphite refining FC 300 $_{(Mo + RG)}$ has, on average, 418 MnS/mm² particles, in which 27% of the inclusions measured in the sample have areas between 11 and 20 µm². On the other hand, 21% of the particles have areas between 6 and 10 µm², and less than 6 µm² represents about 13% of total inclusions, as shown in Fig. 4b.

The FC 250 presented 391 MnS/ mm^2 particles, with 33% of inclusions having areas between 11 and 20 µm², 20% of the particles having areas between 6 and 10 µm², and 7% of inclusions having areas between 1 and 5 µm². The FC 300 $_{(Mo)}$ has, on average, 351 MnS/mm² particles that are present in the material as follows: 25% of the analyzed particles have areas between 11 and 20 µm², 24% of the inclusions have areas between 6 and 10 µm² and only 5% of the MnS particles have areas smaller than 6 µm². To check if there are statistically significant differences in the number of inclusions per square millimeter among the three materials, an analysis of variance (ANOVA) was carried out regarding the average amount of MnS/mm^2 particles. Table 6 shows the results of the analysis of variance for the average amount of MnS particles / mm^2, while Table 7 shows the results of the analysis of the distribution of the areas of the MnS particles.

Table 6
Result of the analysis of variance for the average amount of MnS particles / mm^2.

Analysis of variance for quantity average of MnS / mm^2 particles					
Source of Variation	SS	dl	MS	F	P-value
Between Groups	7406,888889	2	3703,444444	122,540441	0,000013
Within Group	181,333333	6	30,222222		
Total	7588,222222	8			

Table 7
Result of the MnS particle area distribution analysis.

Distribution analysis of MnS particle areas					
Source of Variation	SS	dl	MS	F	P-value
Between Groups	14083	3	4694,33333	18,499835	0,008281
Within Group	1015	4	253,75		
Total	15098	7			

The data were obtained using a 95% confidence interval and a 5% significance level using Matlab® software. The analysis of variance (ANOVA) was also used for the cementite interlayer spacing (μm) of the perlite and the size of the MnS particle areas of the materials used in the research.

The results of the pearlite interlayer spacing of the tested materials are shown in Fig. 5. Note that, in terms of average values, the FC 300 $_{(Mo + RG)}$ has the smallest spacing between layers, an average of 0.29 μm. Thus, this factor may have influenced the hardness of this material, which was greater than the FC 300 $_{(Mo)}$ and FC 250 (Table 3). The variance (ANOVA) analysis was used to confirm a significant difference between the material's interlayer spacing (μm). Table 8 shows the results of the analysis of variance for interlayer spacing (μm). It can indicate that, for gray cast iron with molybdenum and graphite refining, there will be an increase in tensile strength and abrasiveness, thus lowering the machinability.

Table 8
Result of the analysis of variance for interlayer spacing (μm).

Source of Variation	SS	dl	MS	F	P-value
Between Groups	0,065664	3	0,021888	17,315181	0,009353
Within Group	0,005056	4	0,001264		
Total	0,070721	7			

3.2 Tool life and wear mechanisms

Figure 6 illustrates the average results for the tool life of the evaluated materials for the cutting conditions shown in Table 5. The results were interpolated to a VB_{Bmax} = 0.4 mm, using the methodology proposed by da Silva, et al. [12]. Based on the results, it is observed that the FC 250 presented the best machinability among the analyzed materials, the explanation being that its mechanical properties are inferior compared to the other analyzed materials, as shown in Table 3. To show statistical differences between all materials, an analysis of variance (ANOVA) with 95% reliability was performed according to the values illustrated in Fig. 6, with the result in Table 9. Based on these results, it is observed that all input variables significantly influenced the process, with the cutting speed the variable with the most significant influence and the type of material the variable with the lowest.

Table 9
Analysis of variance for the tool life.

Effect	SS	DoF	MS	F	p
Intercept	10223.74	1	10223.74	553.4243	0.000000
Material	563.62	3	187.87	10.1698	0.002211
v_c	870.99	1	870.99	47.1477	0.000044
f	825.27	1	825.27	44.6729	0.000055
Error	184.74	10	18.47		

Figure 7 illustrates the individual effects of each input variable indicated in Table 9 about the machining time. Figure 7a shows a clear relationship between the increase in mechanical properties and the reduction of machinability, similar to that observed by da Silva, et al. [3] in the drilling process of similar materials. Figure 7b illustrates that the increase in cutting speed resulted in a decrease in machinability, which, according to da Silva, et al. [13], is explained for graphitic cast irons by the increase in forces and temperatures at the cutting interface due to the increase in cutting speed. Figure 7c indicates that the increase in feed resulted in a decrease in machinability, which can be explained by the greater volume of material removed by tool interaction resulting in greater forces on the cutting edge [14].

Figure 8 illustrates the combined effects of the material, cutting speed, and feed-on material machinability. This analysis allows us to infer that the most significant differences in machinability between the materials are observed for the lowest speed (v_c = 230 m/min), with the tool life of the materials being similar for the most severe cutting conditions (v_c = 350 m/min, f = 0.2 mm/rev), corroborating the fact that the cutting parameters have a much more significant effect on machinability than the materials evaluated as indicated by the analysis of variance in Table 9. This graph also shows that the FC 250 has machinability considerably superior to the other materials for the lower cutting conditions, confirming the challenge of machining high-strength graphitic cast irons, particularly at higher cutting speeds.

Through an approach similar to that of da Silva, et al. [3], the average machinability (based on the tool lives) values for each material about the parameters indicated in Table 5 were linearly correlated with Table 3 and Fig. 5. Among the variables analyzed, only the macrohardness of the materials was found to have a significant correlation with the machinability of the process, despite the microhardness of the matrix showing a linear correlation of almost 70%.

The more significant correlation of hardness between UTS and interlayer spacing is because hardness is the property that most correlates with the dynamic shear strength of the material for the high shear rates observed in machining [14]. The more significant correlation of Brinell macrohardness about the Vickers microhardness of the matrix can be explained by the greater measurement area of the macrohardness, which also takes into account the influence of graphite on the stress/strain behavior of the material, which according to Collini, et al. [15] is a defining characteristic of the mechanical behavior of graphitic cast irons.

At the end of the tool life tests, the cutting tools were taken to a scanning electron microscope (SEM) to analyze the wear mechanisms of the tools. The predominance of adhesion mechanisms (attrition), microabrasion, and chipping was evident in the machining of the four cast iron alloys, regardless of the cutting conditions tested. Analysis by dispersive energy spectrometry (EDS) detected significant amounts of workpiece material adhered to the worn region of the tool in all tests.

Figure 10 and Fig. 11 illustrate the images obtained by SEM of the worn regions of the tools used in machining the four tested materials, respectively, in the lowest cutting conditions (v_c = 230 m/min and f = 0.1 mm/rev) and the most severe (v_c = 350 m/min and f = 0.2 mm/rev).

It is observed that the flank wear is more pronounced in the most severe conditions, but the wear mechanisms are practically unchanged, concluding that they are only accelerated with higher cutting and feed speeds. When machining compacted graphite cast iron (FV 450) and gray cast iron of a greater resistance (FC 300 $_{(Mo+RG)}$ and FC 300 $_{(Mo)}$), the presence of micro/macro chipping is always observed, while in machining the less resistant gray cast iron (FC 250) chipping does not appear. When machining the FC 250, the photos in Fig. 10d and Fig. 11d show the predominance of the micro-abrasive mechanism. However, considering that in this material, there is no evidence of the presence of precipitates of very high hardness, the micro abrasion must have originated in the particles of the tool itself, lost by attrition (adhesion), leading to the conclusion of the occurrence of this wear mechanism as well [16].

It is observed that the lowest flank wear among all the tests occurred in the cast iron alloy FC 250. According to da Silva, et al. [3], this is due to the high carbon content associated with the lower number of eutectic cells, a higher percentage of broad graphite lamellae, and the lower hardness of this material. Another relevant aspect is the presence of oxygen in the worn surfaces of the tools. This presence indicates that in this region, there was the penetration of atmospheric air and the possible formation of oxides. These oxides adhere to the tool's surface and, subsequently, are pulled out by the flow of workpiece material, interacting in the tribological system to promote adhesive wear during the milling process [17].

3.3. Analysis of roughness of the machined surfaces

Figure 12 illustrates the average roughness (Ra) of the machined surfaces of each material for each cutting condition. Due to the difficulty in finding correlations between machining parameters and the resulting surface roughness, an analysis of variance (ANOVA) was performed for the results illustrated in Fig. 12, with this analysis being illustrated in Table 10. The analysis of variance indicated that for a 95% confidence interval, the variation of the input parameters has no statistical effect on Ra.

Table 10
Analysis of variance for the Ra.

Effect	SS	DoF	MS	F	p
Intercept	2.133133	1	2.133133	134.8657	0.000000
Material	0.058617	3	0.019539	1.2353	0.347674
v_c	0.045422	1	0.045422	2.8718	0.121007
f	0.033079	1	0.033079	2.0914	0.178738
Error	0.158167	10	0.015817		

According to Guesser, et al. [18], the graphite shape significantly impacts the surface finish when machining graphite cast irons. This is due to its stress-concentrating effect dictating the shear mode of the material in the cutting zone and its ejection from the die through the phenomenon known as open grain, directly impacting the roughness of the machined surface. Based on these facts, a new analysis of variance was carried out and illustrated in Table 11, excluding the compacted graphite cast iron, since the presence of vermicular and nodular graphites in it makes the tribosystem at the cutting interface completely different [3].

Table 11
Analysis of variance for the Ra considering only the gray cast irons

Effect	SS	DoF	MS	F	p
Intercept	1.742568	1	1.742568	106.5811	0.000017
Material	0.046424	2	0.023212	1.4197	0.303701
v_c	0.083339	1	0.083339	5.0973	0.048528
f	0.026756	1	0.026756	1.6365	0.241577
Error	0.114448	7	0.016350		

The analysis of variance illustrated in Table 11 indicated that among the input variables analyzed, only the cutting speed presented, for a 95% confidence interval, statistical significance about the roughness of the machined surface. This effect can best be seen in Fig. 13, which illustrates that higher cutting speeds resulted in lower roughness values. The possible explanation for this phenomenon is the fact that higher shear rates due to the higher cutting speed decrease the shear of the material in the primary and secondary shear planes [19], in addition to making graphite ejection difficult in the open-grain phenomenon by decreasing the time that the material remains undergoing plastic deformation with the increase in the shearing rate [20].

In Fig. 14, correlations were drawn between the mechanical properties of the material and the average roughness for all the cut variables evaluated, in a similar way done for the tool life, Fig. 9, but now, only for the gray cast irons. Linear correlations above 70% were observed only for the macroscopic mechanical properties that consider the matrix and graphite, i.e., the tensile strength and Brinell macro-hardness. Since these properties consider the stress concentration of the graphitic phase and its interactions with the material matrix, the overlap of the effects of the phenomena caused by the presence of this second phase on the surface

integrity of the material is evident, i.e., the ejection of the graphite (open grain) and the shear in the cutting zone.

4. Conclusions

This paper studied the tool life, wear mechanisms, and surface roughness in the face milling process of four different graphitic cast irons, for two levels of cutting speed and feed rate. The output variables were compared with the material's mechanical properties, allowing a better understanding of the results. The investigation allowed the following conclusions to be drawn:

• The FC 250 gray cast iron outperformed the other materials in the tool life. This performance, however, was more pronounced for the lower cutting speed and feed tested.

• The compacted graphite cast iron FV 450 presented the poorest machinability about the tool life, however, with results close to the high strength gray cast irons (FC 300 $_{(Mo)}$ and FC 300 $_{(Mo+RG)}$) at the more aggressive cutting conditions.

• The Brinell hardness was the material property that better correlated with the tool life, as it evaluates both the matrix and the graphitic phase of the materials.

• Adhesion (attrition), microabrasion, and microchipping were the prevailing wear mechanisms for all machining conditions tested. The flank wear was more pronounced at the more aggressive cutting conditions.

• The input variables did not show statistical significance on the surface roughness of the evaluated materials. However, when the FV 450 was taken out of consideration, the cutting speed presented statistical significance about the surface Ra.

• Both the UTS and the Brinnel macrohardness are correlated with the surface roughness of the machined surface, as those parameters represent the properties of the matrix and the graphitic phase, which are linked with the shear behavior of the materials.

• Substituting a more resistant material in block engines, for example, is advantageous for the performance of the motor, but this has a price. These more resistant materials (FC 300 $_{(Mo)}$ and FC 300 $_{(Mo+RG)}$) have lower machinability in terms of tool life as compared to the commonly used FC250 gray cast iron but higher than the compact graphite cast iron FV450. The difference tends to reduce when using the more severe cutting conditions (high cutting speed and feed rate). In terms of surface roughness, the same cannot be said; it depends on the cutting conditions. In the more severe cutting conditions tested (v_c = 350 m/min), the more resistant gray cast irons showed better surface roughness than the FC250.

Declarations

Acknowledgements

The authors are grateful to the Brazilian research agencies CNPq, FAPEMIG, and *Coordenação de Aperfeiçoamento de Pessoal de Nível Superior - Brasil* (CAPES) - Finance Code 001 for financial support to

Tupy S.A. for providing the work material and technical support and to Walter for the donation of the tooling.

Funding

The authors declare that no funds, grants, or other support were received during the preparation of this manuscript.

Conflicts of interest/Competing interests

The authors have no relevant financial or non-financial interests to disclose.

Availability of data and material

All the authors declare that this paper has no available data or material.

Code availability

All the authors declare that this paper has no available code.

Ethics approval

All the authors declare that this paper didn't need ethics approval.

Consent to participate

All the authors declare that this paper didn't need consent to participate.

Consent for publication

All the authors declare that all items in this work present consent for publication.

Author Contributions

All authors contributed to the study conception, design, writing, material preparation, data collection, and analysis. All authors read and approved the final manuscript.

References

1. J. Li, P. Wang, X. Cui, K. Li, R. Yi, Gray cast iron cylinder head thermal mechanical fatigue analysis, Proceedings of the FISITA 2012 World Automotive Congress, Springer, 2013, pp. 243-257.
2. L. Da Silva, H. Costa, Maskless electrochemical texturing of automotive cylinders, Materials Performance and Characterization, 6 96-111, 2017.
3. A.E. da Silva, L.R.R. da Silva, A. dos Reis, Á.R. Machado, W.L. Guesser, E.O. Ezugwu, Relationship between mechanical and metallurgical properties with machinability when drilling high-strength cast irons, The International Journal of Advanced Manufacturing Technology, 106 2020.
4. J.R. Davis, ASM specialty handbook: cast irons, ASM International, 1996.
5. H.T. Angus, Cast iron: physical and engineering properties, Elsevier, 2013.

6. K. Odum, N. Raymond, D. Pell, M. Soshi, Surface feature formation mechanism during finish milling of gray cast iron, The International Journal of Advanced Manufacturing Technology, 92 2017.
7. T. S.A., FUCO PERFIS FUNDIDOS, 2019.
8. ASTM, Standard Test Method for Evaluating the Microstructure of Graphite in Iron Castings, 2019.
9. Guesser, W. L. “Propriedades Mecânicas dos Ferros Fundidos”.1. ed. São Paulo: Blüsher, 2009. 336p.
10. Dawson, S. "Compacted graphite iron – A material solution for modern diesel engine cylinder blocks and heads". China Foundry, v. 6, p. 241-246, 2009.
11. G. Vander Voort, A. Roosz, Measurement of the interlamellar spacing of pearlite, metallography, 17 -1984 - 1-17.
12. ISO, Geometrical Product Specifications (GPS) — Surface texture: Profile method — Rules and procedures for the assessment of surface texture, 2019.
13. L. da Silva, V. Del Claro, C. Andrade, W. Guesser, M. Jackson, A. Machado, Tool wear monitoring in the drilling of high-strength compacted graphite cast irons, Proceedings of the Institution of Mechanical Engineers, Part B: Journal of Engineering Manufacture, 2020.
14. L.R.R. da Silva, A.F. Filho, E.S. Costa, D.F. Marcucci Pico, W.F. Sales, W.L. Guesser, A.R. Machado, Cutting Temperatures in End Milling of Compacted Graphite Irons, Procedia Manufacturing, 26, 2018, 474-484.
15. V.P. Astakhov, Tribology of metal cutting, Elsevier, 2006.
16. L. Collini, G. Nicoletto, R. Konečná, Microstructure and mechanical properties of pearlitic gray cast iron, Materials Science and Engineering: A, 488, 2008- 529-539.
17. L. da Silva, F. Souza, W. Guesser, M. Jackson, A. Machado, Critical assessment of compacted graphite cast iron machinability in the milling process, Journal of Manufacturing Processes, 56,2020, 63-74.
18. S. Dawson, I. Hollinger, M. Robbins, J. Daeth, U. Reuter, H. Schulz, The effect of metallurgical variables on the machinability of compacted graphite iron, SAE transactions, 2001 334-352.
19. W.L. Guesser, F.S. Pereira, L. Boehs, Surface changes during turning of grey cast iron, International Journal of Machining and Machinability of Materials, 18 ,2016 - 313-324.
20. S. Thamizhmanii, S. Hasan, Analyses of roughness, forces and wear in turning gray cast iron, Journal of achievement in Materials and Manufacturing Engineering, 17, 2006.
21. P.W. "Materials, Effects of austempering process on mechanical behavior properties of compacted graphite iron", 2019.
22. AN Overview Prachl Singhal, Kuldeep K. Saxena, "Effect of silicon addition on microstructure and mechanical properties of grey cast Iron", Department of Mechanical Engineering, GLA University, Mathura, UP, 281406, India, 2020.
23. G. Goodrich, Case histories of cast iron machinability problems, Modern casting, 87-1997. 30-33
24. Johnson O. Agunsoye[1], Talabi S. Isaac[2], Olumuyiwa I. Awe[3], Afemefuna T. Onwuegbuzie[1] "Effect of Silicon Additions on the Wear Properties of Grey Cast Iron" [1]Department of Metallurgical and Materials Engineering, University of Lagos, Lagos, Nigeria, [2]Department of Materials and Metallurgical Engineering, University of Ilorin, Ilorin, Nigeria,[3]Department of Metallurgical Engineering, Yaba College of Technology, Lagos, Nigeria, 2013.

25. Janowak and Gundlach, "A modern approach to alloying gray Iron", AFS, Vol.90, 1982, pp 847-862.
26. Rosenthal, "Theory of metal casting", TMH Co. Ltd., 1990, pp 23,607.
27. *Walter, L.* Seelbach. "The Gray *Iron Castings Handbook",* Iron Castings Society", INCO, pp 21, 146, 206, 208.
28. Cupola Hand Book, 5th Edition, AFS Publications, 2014, pp 365-378.
29. Molybdenum Steels Irons Alloys, Climax Molybdenum Company, 2014, pp 15-16, 42, 52, 288-304.
30. A.B. Mohd Hadzley[1], M.R. Nurul Fatin[1], R.A. Raja Izamshah[1], N.I.S. Hussein[1], A. Siti sarah[1], e and S. Sivarao[1], "Surface Integrity of a High-Speed Milling FC300 Gray Cast Iron" Faculty of Manufacturing Engineering, Universiti Teknikal Malaysia Melaka (UTeM), Hang Tuah Jaya, 76100 Durian Tunggal, Melaka, Malaysia, 2014.
31. K. Hato, S. Kazuhiro and S. Hitoshi, "Cutting performance of a binder-less sintered cubic boron nitride tool in the high-speed milling of grey cast iron", Journal of Material Processing Technology. 127 217-221 - 2002.
32. R. Elliott, "Cast Iron Technology" Butterworths & co. (publishers) Ltd. United Kingdom 1988.
33. Y. Sahin and A.R. Motorcu, "Surface roughness model in machining hardened steel with cubic boron nitride cutting tool", International Journal of Refractory Metals & Hard Metal. 26 84- 90 -2008.
34. De Souza JR. A, M, Sales, W.F, Santos S.C, Machado, A.R "Performance of single Si3N4 and mixed Si3N4+ PCBN wiper cutting tools applied to high speed face milling of cast iron". Int J Mach Tools Manuf 45(3):335–344 – 2005.
35. Yigit R, Celik E, Findik F, Koksal. S, "Effect of cutting speed on the performance of coated and uncoated cutting tools in turning nodular cast iron". J Mater Process Tech 204(1):80–88, 2008.
36. ASTM A247, "Standard Test Method for Evaluating the Microstructure of Graphite in Iron Castings", 2010.
37. Voort, G. F. V.; Roosz, A. "Measurement of the Interlamellar Spacing of Pearlite". Metallography, v. 17, pp. 1-17, 1984.
38. A. Richetti, A. Machado, M. Da Silva, E. Ezugwu, J. Bonney, Influence of the number of inserts for tool life evaluation in face milling of steels, International Journal of Machine Tools and Manufacture, 44 695-700, 2004.
39. ABNT NBR ISO 4288 – "Especificações geométricas de produto (GPS) - Rugosidade: Método do perfil - Regras e procedimentos para avaliação de rugosidade", 2008.
40. Doré, C. "Influência da Variação da Nodularidade na Usinabilidade do Ferro Fundido Vermicular". Dissertação (Mestrado em Engenharia Mecânica) – Departamento de Engenharia Mecânica, Universidade Federal de Santa Catarina, Florianópolis, 2007.
41. Xavier, F. A. "Aspectos Tecnológicos do Torneamento do Ferro Fundido Vermicular com Ferramentas de Metal-duro, Cerâmica e CBN". Dissertação (Mestrado em Engenharia Mecânica) – Departamento de Engenharia Mecânica, Universidade Federal de Santa Catarina, 2003.
42. König, W.; Klocke, F. Fertigungsverfahren: Drehen, Frasen und Bohren. Berlim: Heidelberg, 2008. p. 562.
43. Machado, Á. R.; Abrão, A. M.; Coelho, R. T.; Da Silva, M. B. "Teoria da Usinagem dos Materiais". 3. ed. São Paulo – SP: Edgard Blücher, 2015. p. 407.
44. Reuter, U., Schulz, H., Dawson, S., Hollinger, I., Robbins, M., Daeth, J. "The Effect of Metallurgical Variables on the Machinability of Compacted Graphite Iron". Society of automotive engineers, Inc, Alemanhã, 2001,

p 1-18.

45. Bagetti, J. H. “Análise da Usinabilidade, Deformação e Temperatura no Fresamento dos Ferros Fundidos Vermicular e Cinzento”. Dissertação (Mestrado em Engenharia Mecânica) – Departamento de Engenharia Mecânica, Universidade Federal de Santa Catarina, 2009.
46. Guenza, J.E. “Análise do Desempenho do Fresamento em Altas Velocidades de Corte do Ferro Fundido GG25 em Aplicação Industrial” Dissertação (Mestrado em Engenharia) - Programa de Pós-graduação em Engenharia Mecânica e de Materiais, Universidade Tecnológica Federal do Paraná, Curitiba, 134 p. 2008.
47. Oliveira, J. M. “Caracterização da Integridade de Superfícies Usinadas Para Produção de Moldes e Matrizes”- Pró-reitora de Pós-graduação e Pesquisa Coordenadoria de Pós-graduação Programa de Pós-graduação em Materiais - Universidade de Caxias do Sul-Caxias do Sul. RS 2006.
48. ASM. "Speciality Handbook: Cast Irons",Estados Unidos: ASM International, 1996, p. 33-267.

Figures

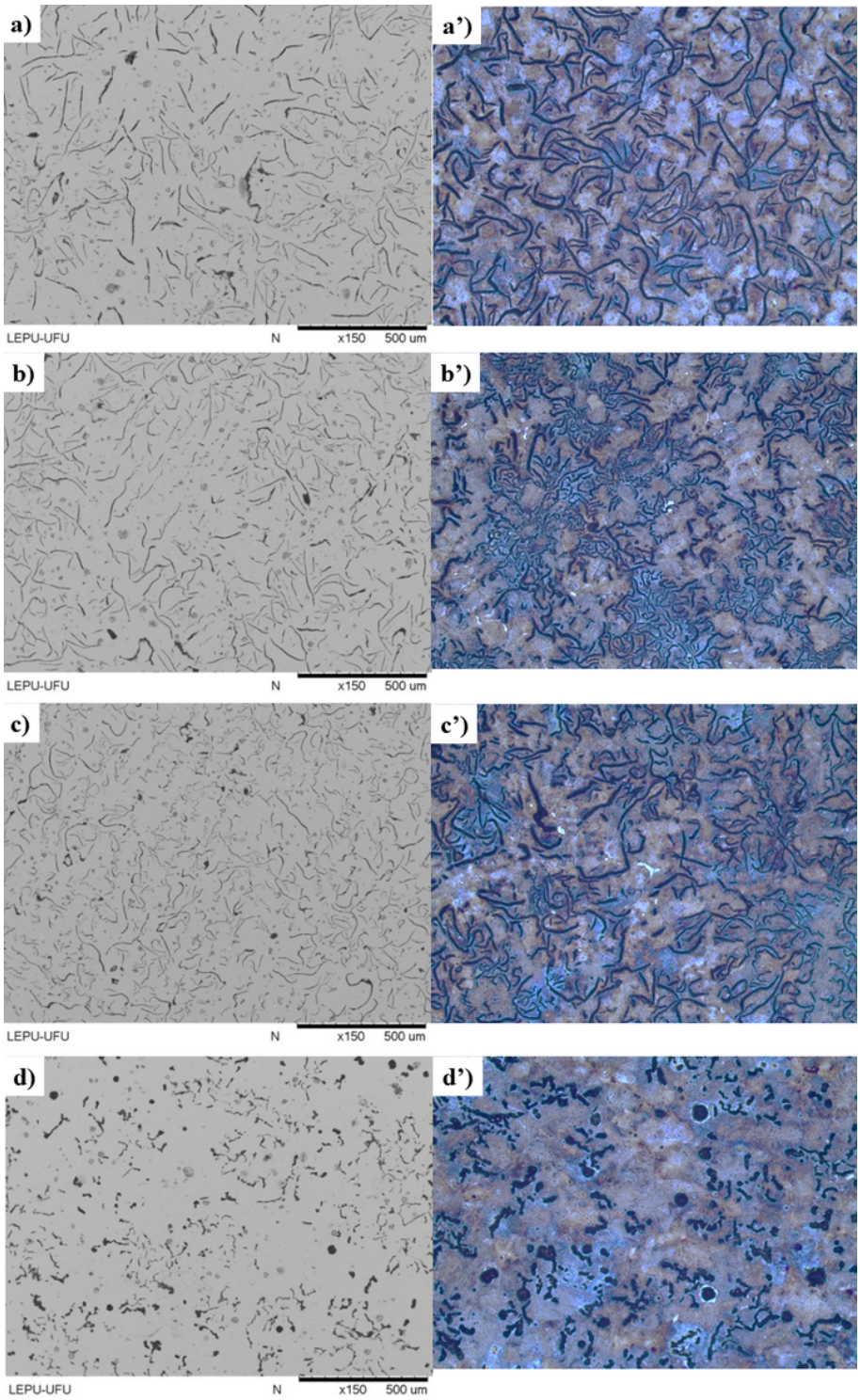

Figure 1

Micrographs of material surfaces with and without 3% Nital attack, obtained by scanning electron microscope (SEM) and optical microscope: a) FC 250; b) FC 300 $_{(Mo)}$; c) FC 300 $_{(Mo+RG)}$; d) FV450.

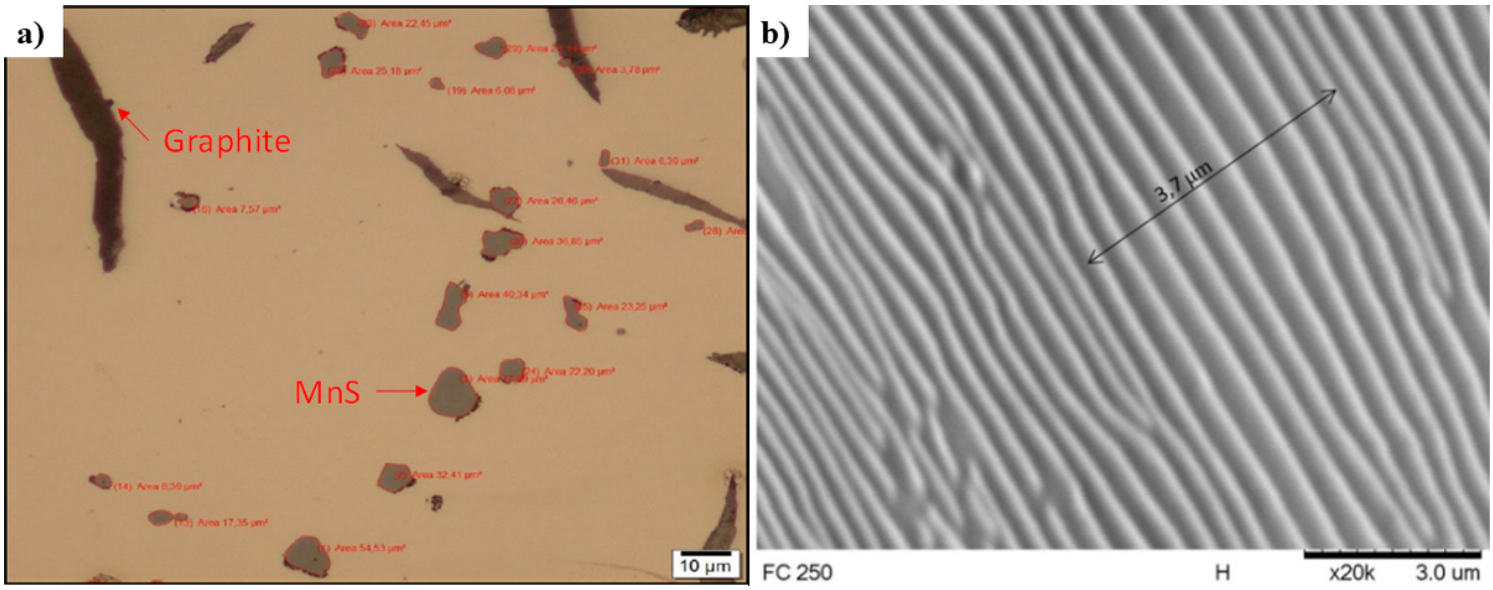

Figure 2

a) Identification of MnS inclusions; b) Determination of the cementite interlayer spacing of the perlite.

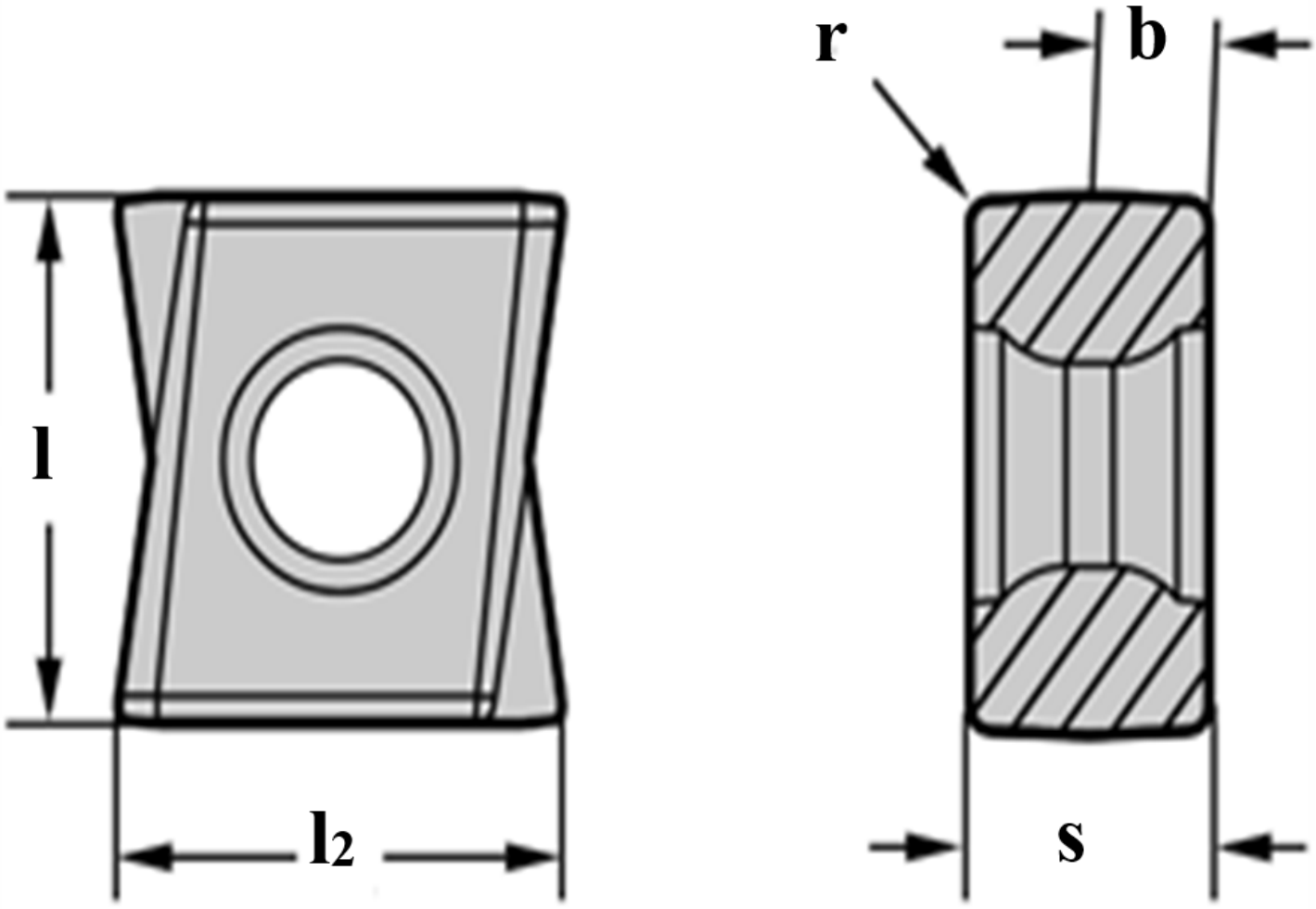

Figure 3

The geometry of the tool used in the tests.

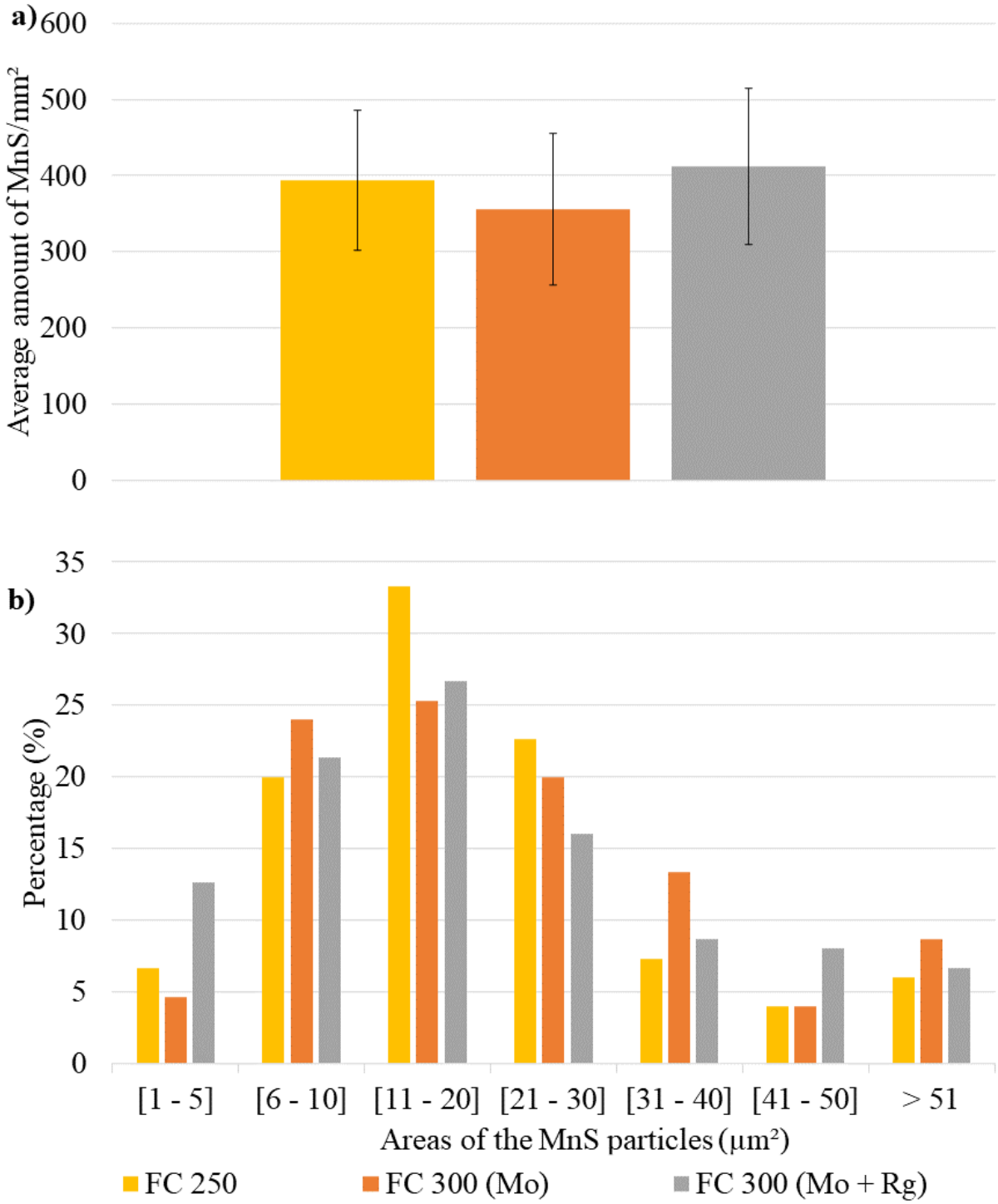

Figure 4

(a) Average amount of MnS/mm² in gray cast iron. (b) MnS particle size distribution in gray cast iron.

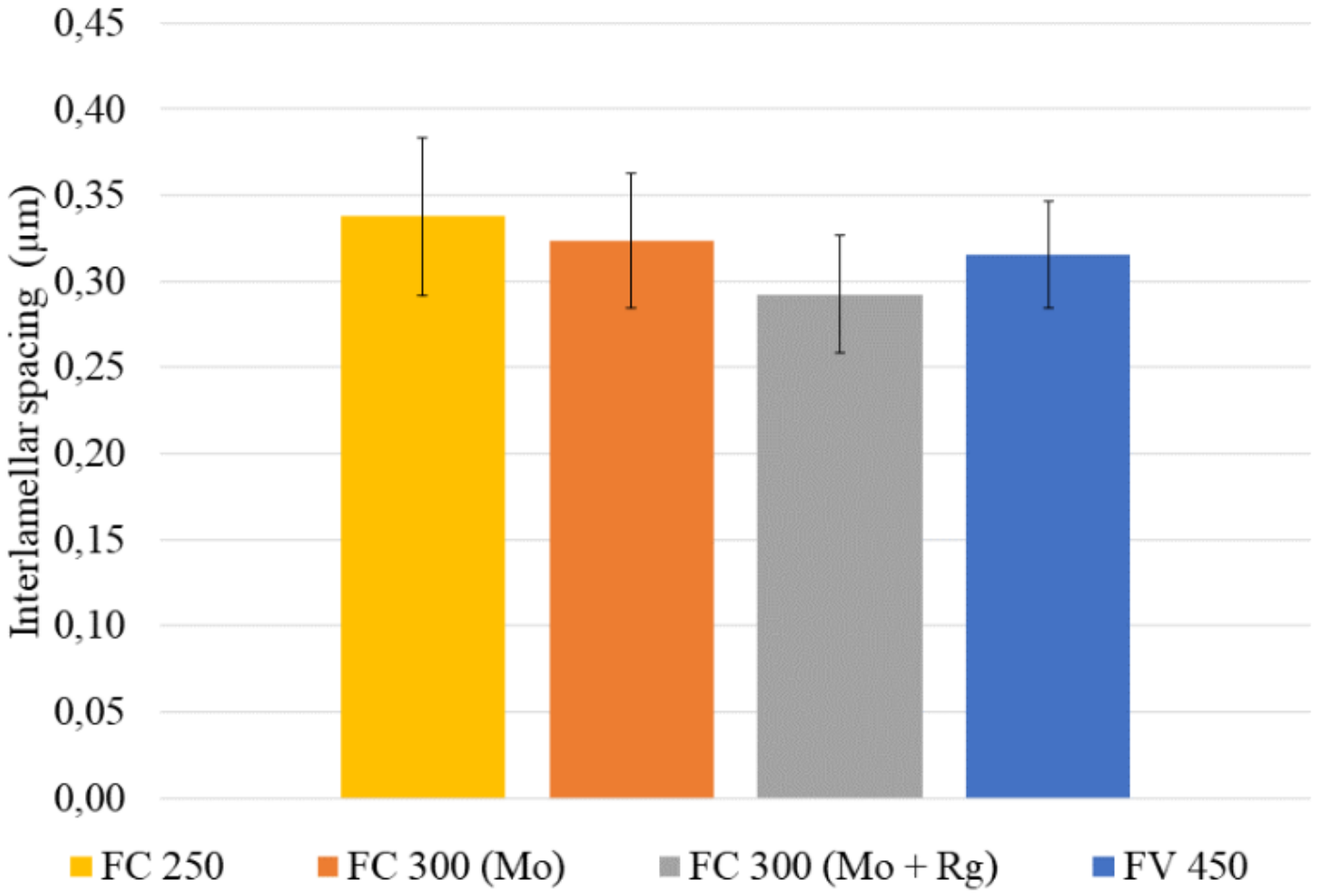

Figure 5

Pearlite interlayer spacing.

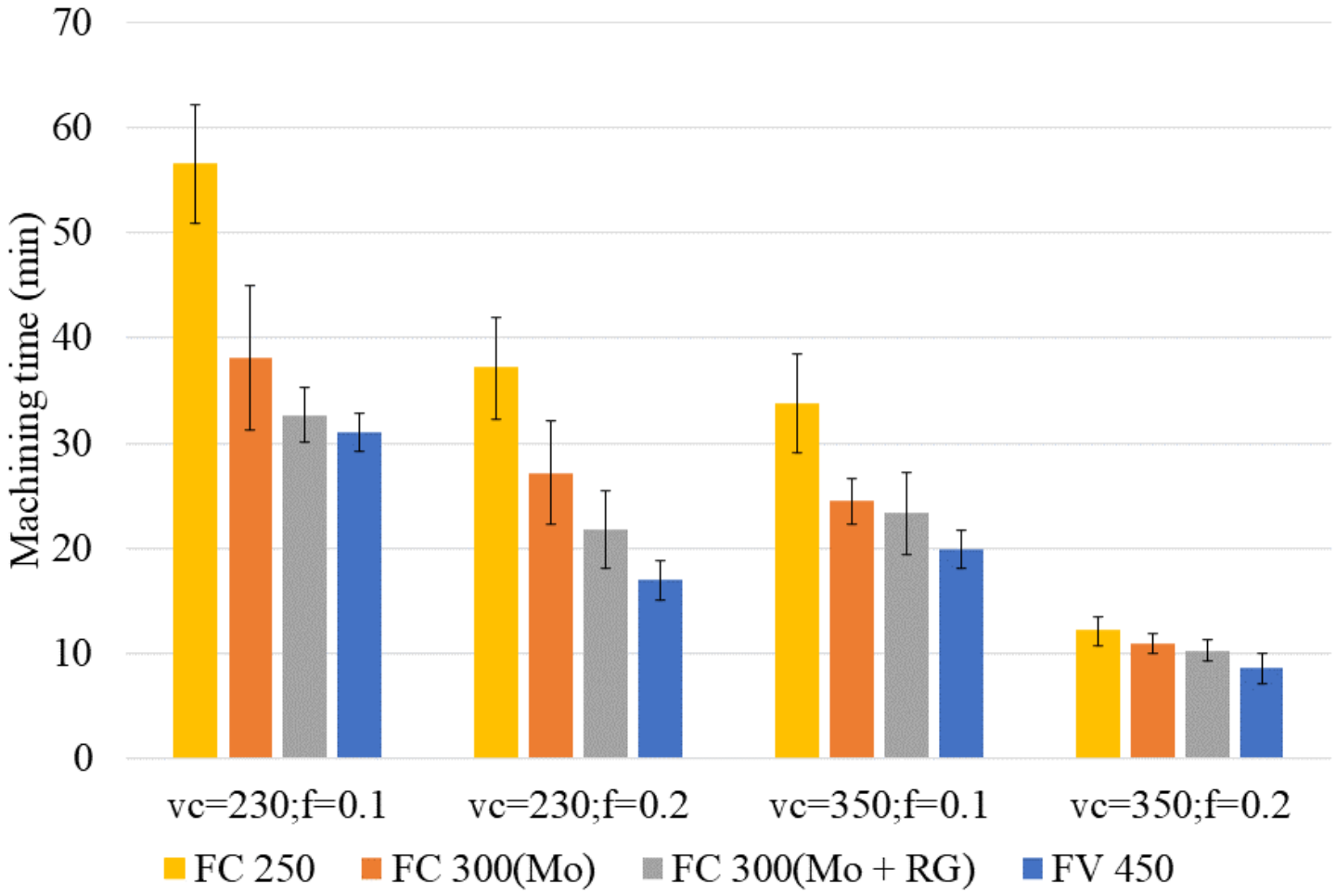

Figure 6

Maximum flank wear (VB_{Bmax}) about Tool life, interpolated for a VB_{Bmax} = 0.4 mm.

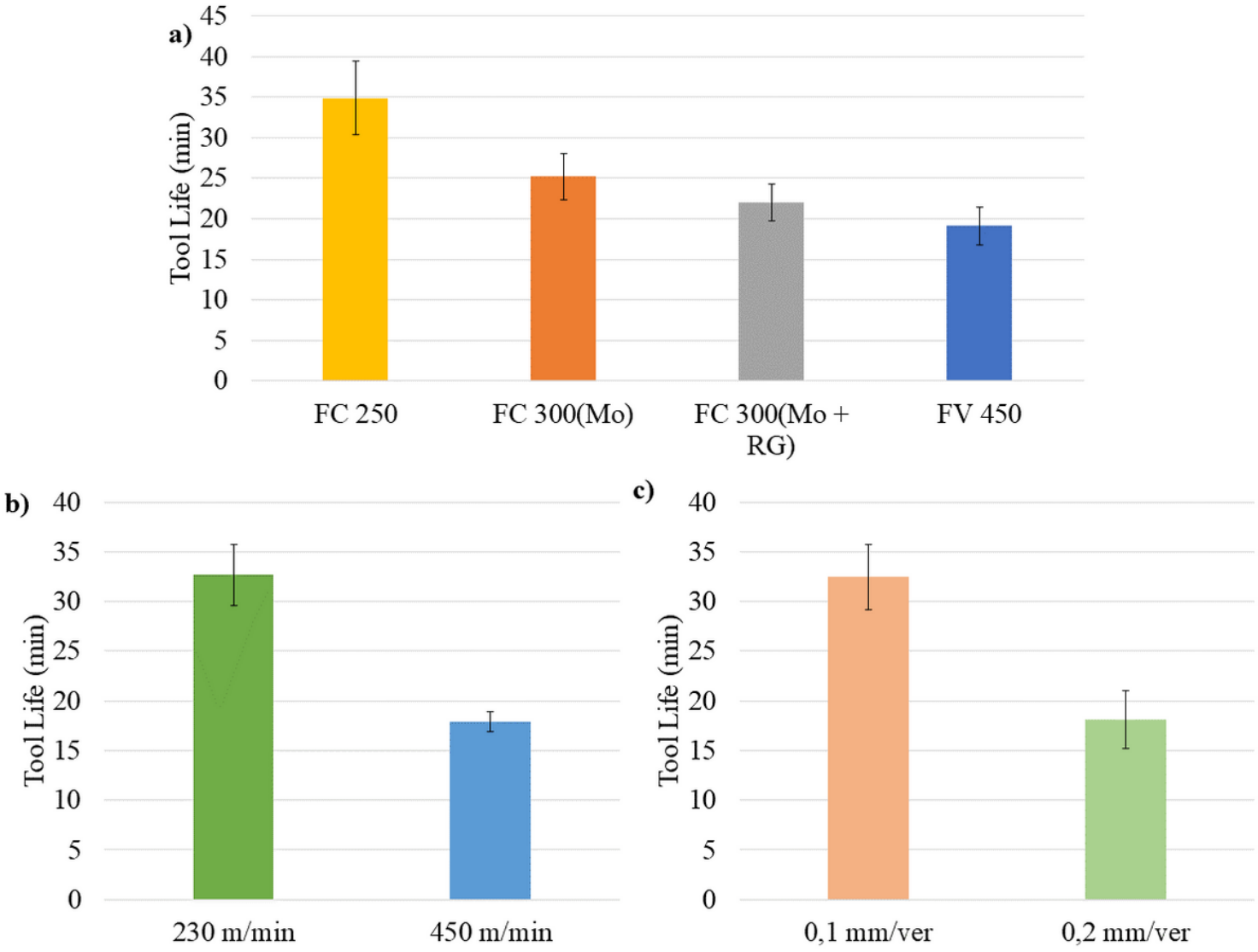

Figure 7

Effects of the test variables in the tool life. (a) material; (b) cutting speed; (c) feed rate.

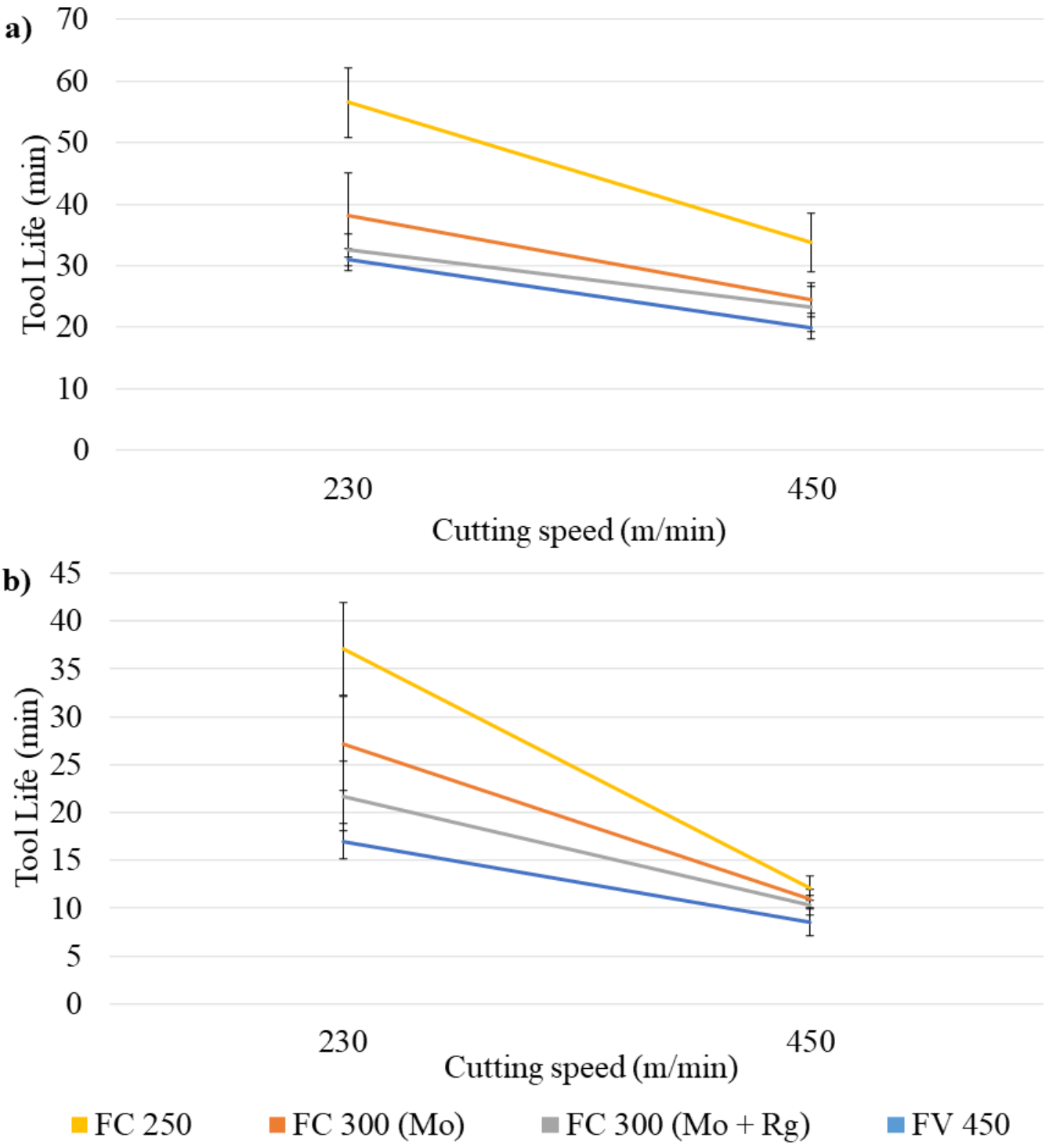

Figure 8

Combine the effects of the machined material and cutting speed in relation to the tool life for (a) f = 0.1 mm/rev; f = 0.2 mm/rev.

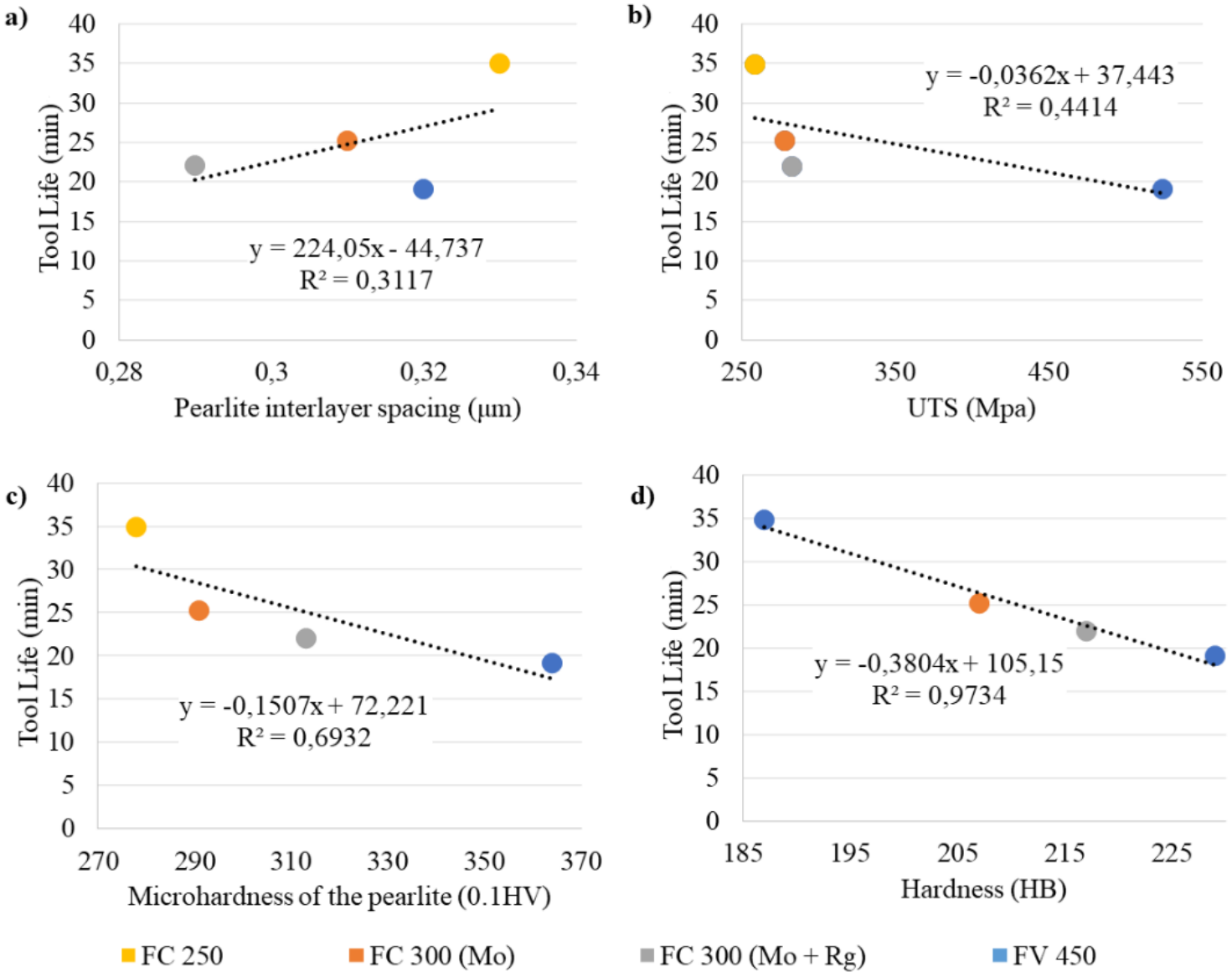

Figure 9

Correlations between mechanical properties and the overall machinability of the tool life, interpolated for a VB_{Bmax} = 0.4 mm. (a) Pearlite interlayer spacing; (b) Ultimate tensile strength; (c) Microhardness of the pearlite; (d) Brinell hardness.

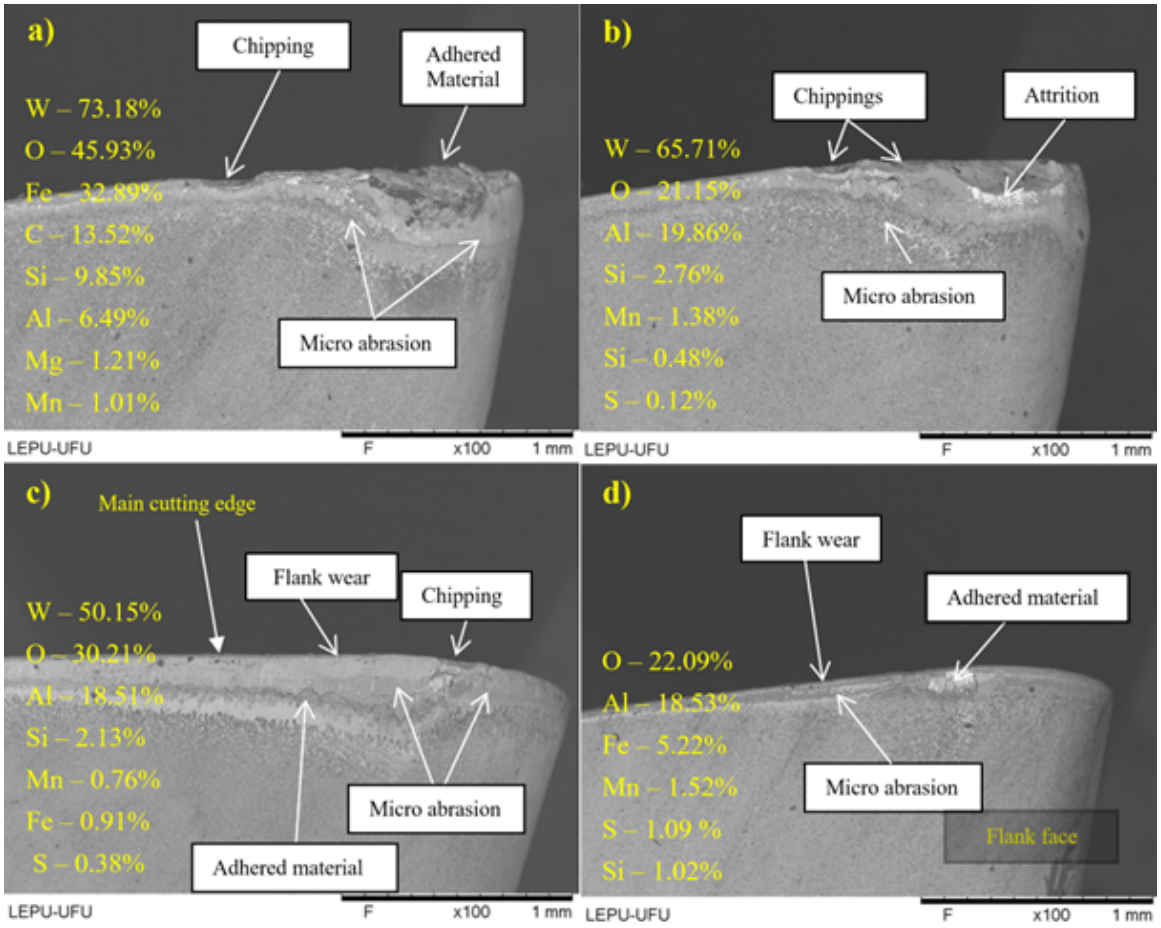

Figure 10

View of the rake surfaces of the tools used at cutting speed v_c = 230 (m/min) and feed per rev f = 0.1 (mm/rev): a) FV 450; b) FC 300 $_{(Mo+RG)}$; c) FC 300 $_{(Mo)}$; d) FC 250.

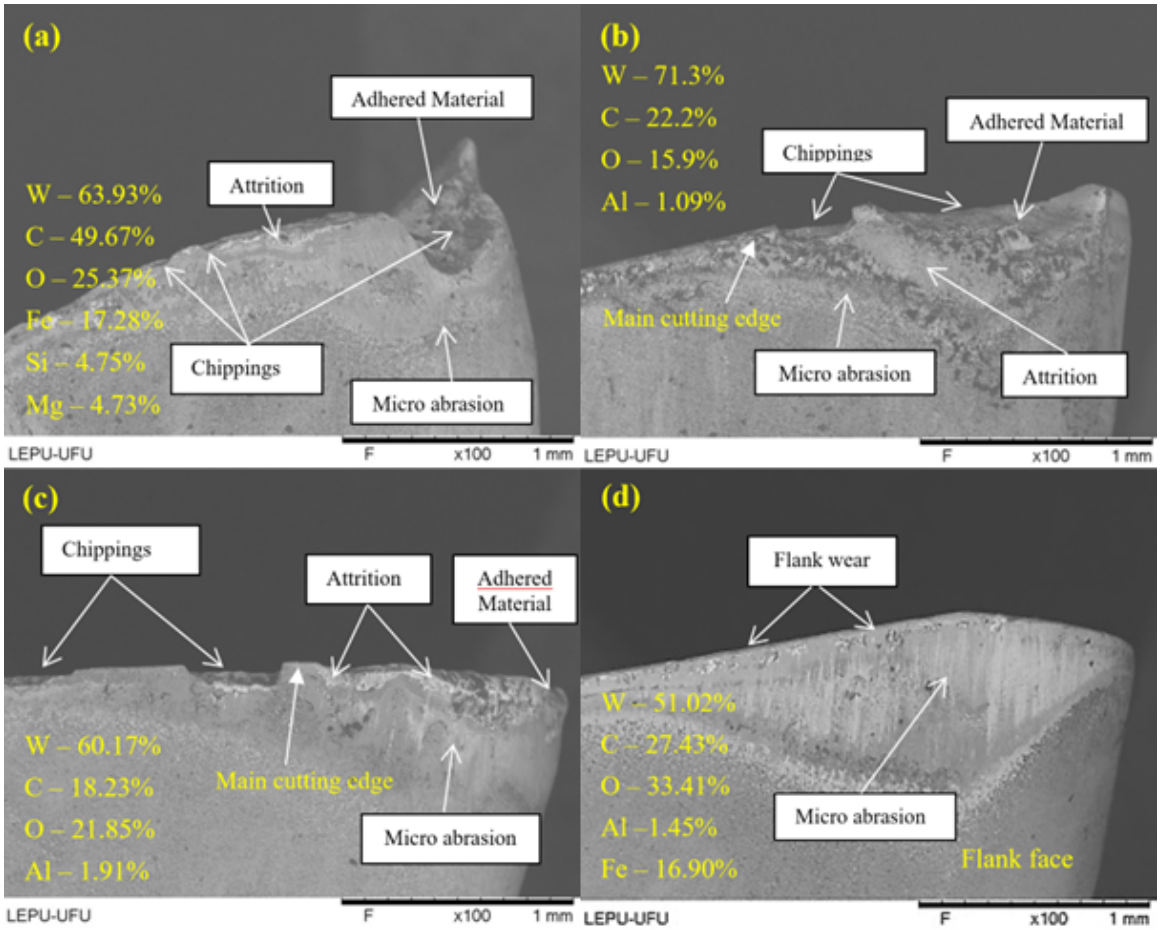

Figure 11

View of the rake surfaces of the tools used at cutting speed v_c = 350 (m/min) and feed per rev f = 0.1 (mm/rev): a) FV 450; b) FC 300 $_{(Mo+RG)}$; c) FC 300 $_{(Mo)}$; d) FC 250.

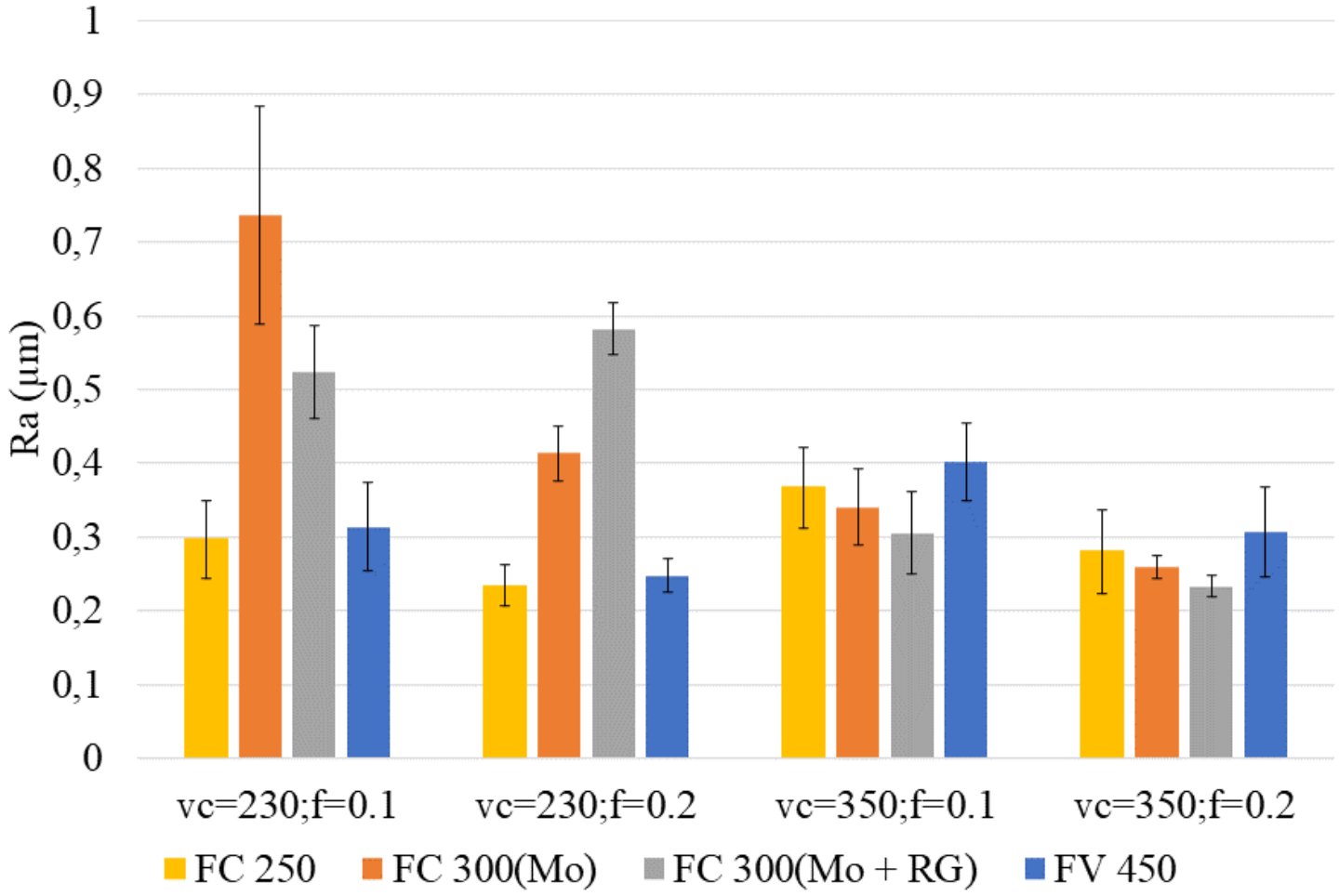

Figure 12

Average roughness profile of the machined surface.

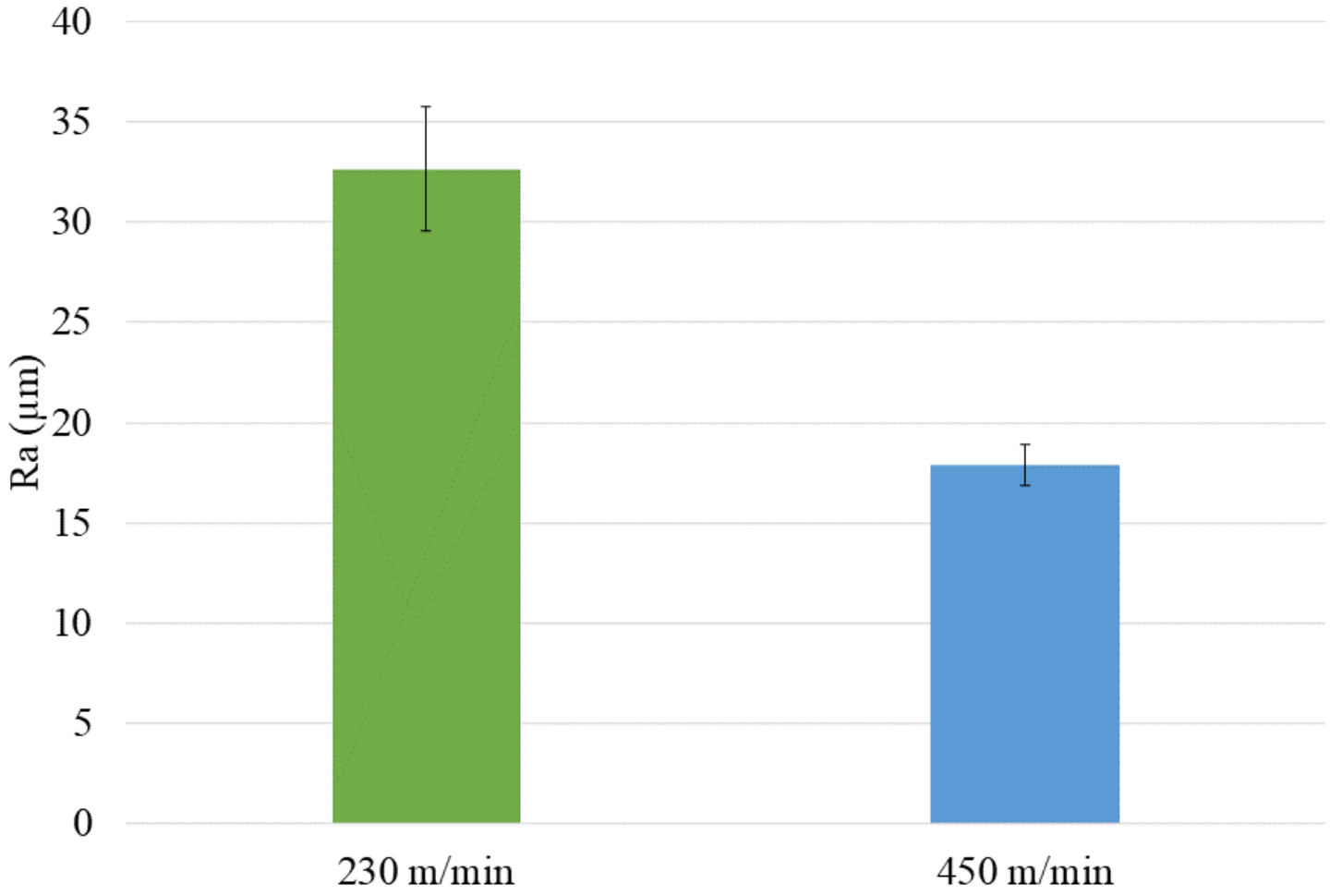

Figure 13

Effects of the cutting speed in the Ra.

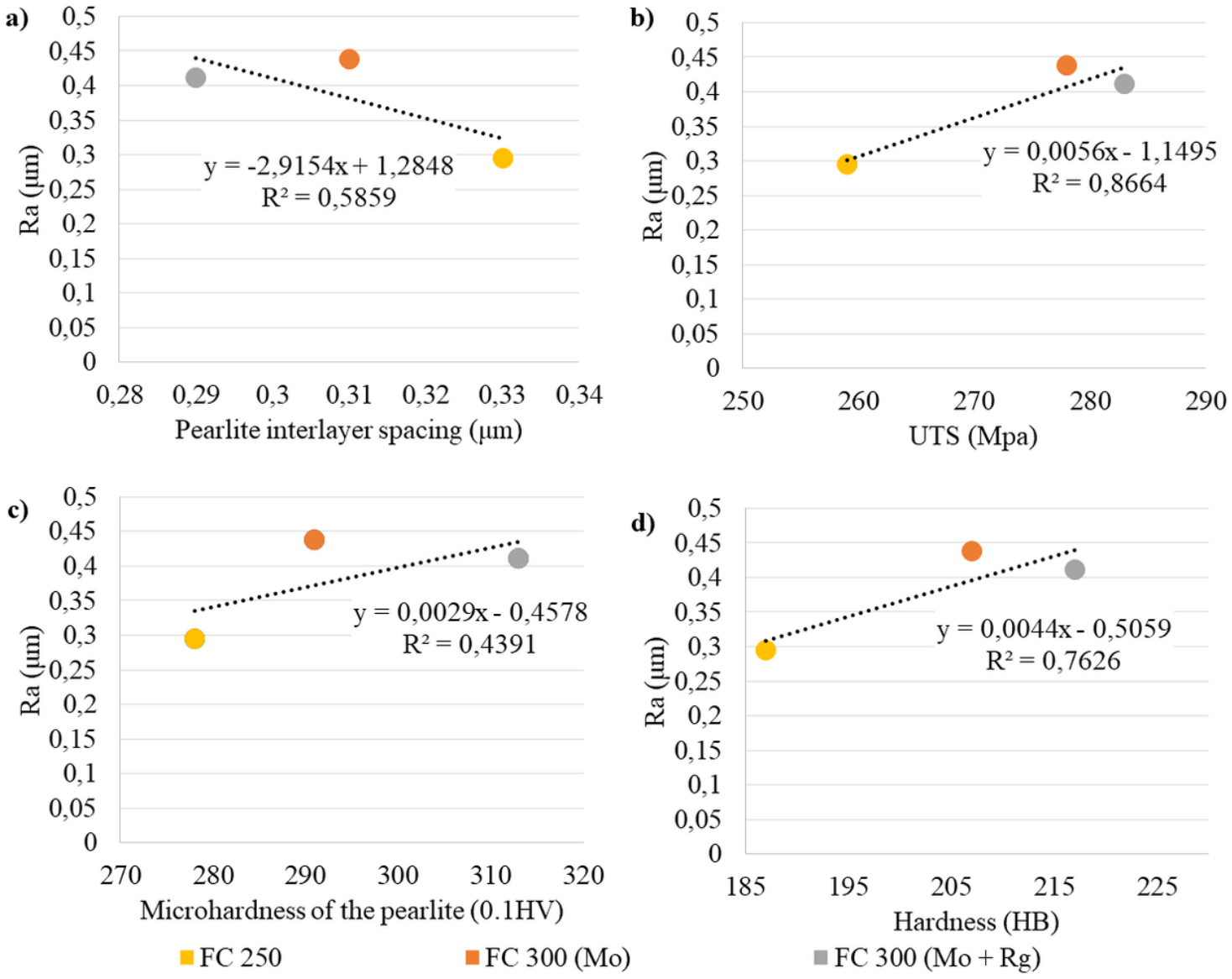

Figure 14

Effect of the material's parameters on the roughness of the machined surface (a) Pearlite interlayer spacing; (b) Ultimate tensile strength; (c) Microhardness of the pearlite; (d) Brinell hardness.